The parallel-sequential field subtraction technique for coherent nonlinear ultrasonic imaging

OPEN ACCESS
IOP Publishing
Smart Materials and Structures
Smart Mater. Struct. **27** (2018) 065002 (10pp)
https://doi.org/10.1088/1361-665X/aabcb2

The parallel-sequential field subtraction technique for coherent nonlinear ultrasonic imaging

Jingwei Cheng, Jack N Potter and Bruce W Drinkwater

Department of Mechanical Engineering, University of Bristol, Queen's Building, University Walk, Bristol BS8 1TR, United Kingdom

E-mail: jingwei.cheng@bristol.ac.uk

Received 31 January 2018, revised 28 March 2018
Accepted for publication 9 April 2018
Published 3 May 2018

Abstract

Nonlinear imaging techniques have recently emerged which have the potential to detect cracks at a much earlier stage than was previously possible and have sensitivity to partially closed defects. This study explores a coherent imaging technique based on the subtraction of two modes of focusing: *parallel*, in which the elements are fired together with a delay law and *sequential*, in which elements are fired independently. In the parallel focusing a high intensity ultrasonic beam is formed in the specimen at the focal point. However, in sequential focusing only low intensity signals from individual elements enter the sample and the full matrix of transmit-receive signals is recorded and post-processed to form an image. Under linear elastic assumptions, both parallel and sequential images are expected to be identical. Here we measure the difference between these images and use this to characterise the nonlinearity of small closed fatigue cracks. In particular we monitor the change in relative phase and amplitude at the fundamental frequencies for each focal point and use this nonlinear coherent imaging metric to form images of the spatial distribution of nonlinearity. The results suggest the subtracted image can suppress linear features (e.g. back wall or large scatters) effectively when instrumentation noise compensation in applied, thereby allowing damage to be detected at an early stage (c. 15% of fatigue life) and reliably quantified in later fatigue life.

Keywords: nonlinear coherent imaging, fatigue crack growth, ultrasonic phased array, noise compensation

(Some figures may appear in colour only in the online journal)

Introduction

Nonlinear ultrasonic methods are sensitive to the micro-structural material changes which precede macroscopic crack growth [1, 2]. As cracks initiate and start to grow, non-classical nonlinearity becomes the dominant feature and leads to a measurable nonlinearity prior to the formation of the large volumetric defects, which may then be detected effectively by conventional linear ultrasonic inspection. This non-classical nonlinearity is described as a contact-acoustic nonlinearity or clapping nonlinearity, which in the simplest case describes the ability of a partially contacting interface to transmit only the compressive component of a wave [3–5]. Recently, several techniques which implement harmonic generation and frequency modulation using ultrasonic transducers to measure elastic nonlinearity have demonstrated the capability to spatially isolate fatigue cracks and effectively monitor their early growth [6–10]. The use of complicated bespoke setups and the lack of robust quantification of measurement errors have led to a significant gap between laboratory results and application by industry [11–18].

Recently, some nonlinear imaging techniques using ultrasonic phased arrays have emerged with the ability to localise and size closed cracks. These techniques can broadly be classified into three groups. Firstly, subharmonic imaging [19] which is conceptually similar to conventional linear array imaging, but which evaluates the subharmonic rather than fundamental component of the received signals. These methods are well suited to imaging of closed cracks since subharmonic generation is associated only with the defect and not nonlinearity of the bulk material or instrumentation. Secondly, an approach, referred to as amplitude modulation, evaluates the nonlinear amplitude dependence of the fundamental frequency component backscattered from the inspection point. Amplitude modulation at the inspection point has been achieved in two ways; by modulating the transmission amplitude [20] and by changing the number of transmitting elements [21]. In the latter technique the scattered amplitude from transmission of all elements simultaneously is subtracted from that recorded using just the odd and even subsets of the elements. Such methods have been shown to increase detectability of closed cracks but imperfectly suppress linear scattering features in the resultant images. Thirdly, nonlinear diffuse energy imaging [22] contrasts the statistical diffuse energy of fields produced by sequential and parallel transmission focusing. Whilst this approach has shown high sensitivity in some cases, when the test structures become large in size or are made of highly attenuating materials, a measurable diffuse field cannot be produced thereby limiting the applicability. Such applications necessitate the use of coherent field imaging methods such as subharmonic scattering and amplitude modulation.

In the present paper, a form of amplitude modulation imaging is explored which is shown to have distinct advantages over the above discussed methods. An ultrasonic phased array is used to create a spatial map of nonlinearity by applying the process of parallel and sequential field subtraction (i.e. as used in nonlinear diffuse energy imaging), to the coherently scattered components of the field at the fundamental frequency. In parallel focusing the elements are fired with a pre-set delay law to cause a high intensity focus at the target pixel. In sequential focusing individual elements are fired in-turn and the full matrix of transmit-receive data is captured and synthetically focused at the pixel location in post-processing. The two resulting images would be linearly equivalent and therefore any differences in phase and amplitude can be attributed to nonlinearity. Hence, the proposed imaging metric here is the difference in coherently scattered amplitude for fields yielded from sequential and parallel focusing at each pixel location. In addition, effects arising from the nonlinearity inherent in the instrumentation are observed in the residual relative phase and amplitude at damage-free points. Processing is applied to remove these effects, greatly improving the suppression of linear scattering features. It is demonstrated that this method can be used to detect fatigue crack growth from 15% of fatigue life in mild steel specimens. In addition, since physical focusing is only required once per pixel, this nonlinear coherent imaging (NCI) approach can shorten the time for data acquisition compared to previous nonlinear amplitude-modulation imaging methods [20, 21], which potentially allows the faster imaging of large structures.

Sequential and parallel fields

Two alternative modes of image formation are commonly employed with a typical commercially available array controller. In parallel transmission mode, all elements are fired near simultaneously in a pre-set sequence termed a delay law. The application of this mode results in a high intensity beam forming in the test structure which is then physically translated, steered or focused to form an image. Alternatively, in sequential mode each transmitter is fired independently and the time-domain signals from all the individual combinations of transmitter-receiver pairs are captured one after the other forming the so-called full matrix of inter-element responses. This full matrix can then be post-processed with the same delay laws used in parallel transmission. If the system is time invariant and the principle of linear superposition holds, these two modes of operation form linearly equivalent responses. However, elastic nonlinearity leads to differences in the fields produced by these two modes of focusing. This difference can be exploited to allow the measurement of material nonlinearity. It has been shown that elastic nonlinearity produces differences in the statistical diffuse energy of parallel and sequentially focused fields and this principle has been used to image fatigue cracks with the nonlinear diffuse energy method [22, 23]. The first part of the present study examines the effect of the nonlinear elastic response of fatigue cracks on the relative properties of the coherently scattered components of the parallel and sequential fields.

Assuming $f_{n,m}(t)$ are the time-domain received signals for each combination of transmit (n) and receive (m) elements in the sequential case. $\delta_n^T(r)$ and $\delta_m^R(r)$ are the transmission delay and the reception delay respectively applied to the nth and mth elements respectively to achieve a focus at a point, $r(x, z)$, which can be expressed as $\delta_n^T(r) = \dfrac{\sqrt{(x_n - x)^2 + z^2} - \sqrt{(x_a - x)^2 + z^2}}{c}$ and $\delta_m^R(r) = \dfrac{\sqrt{(x_m - x)^2 + z^2} - \sqrt{(x_b - x)^2 + z^2}}{c}$, where c denotes the longitudinal wave velocity of the material, x_a and x_b are the positions of reference elements in x-axis for the transmission and reception delay laws respectively. Further, if $g_m(r, t)$ is the time-domain signal received on element m for the parallel transmission of all elements delayed independently by $\delta_n^T(r)$ then the frequency (ω) domain versions of $f_{n,m}(t)$ and $g_m(r, t)$ are given by $F_{n,m}(\omega) = \int_0^{t_r} f_{n,m}(t)\mathrm{e}^{-\mathrm{i}\omega t}\mathrm{d}t$ and $G_m(\omega) = \int_0^{t_r} g_m(t)\mathrm{e}^{-\mathrm{i}\omega t}\mathrm{d}t$, respectively, where t_r is the reception end time.

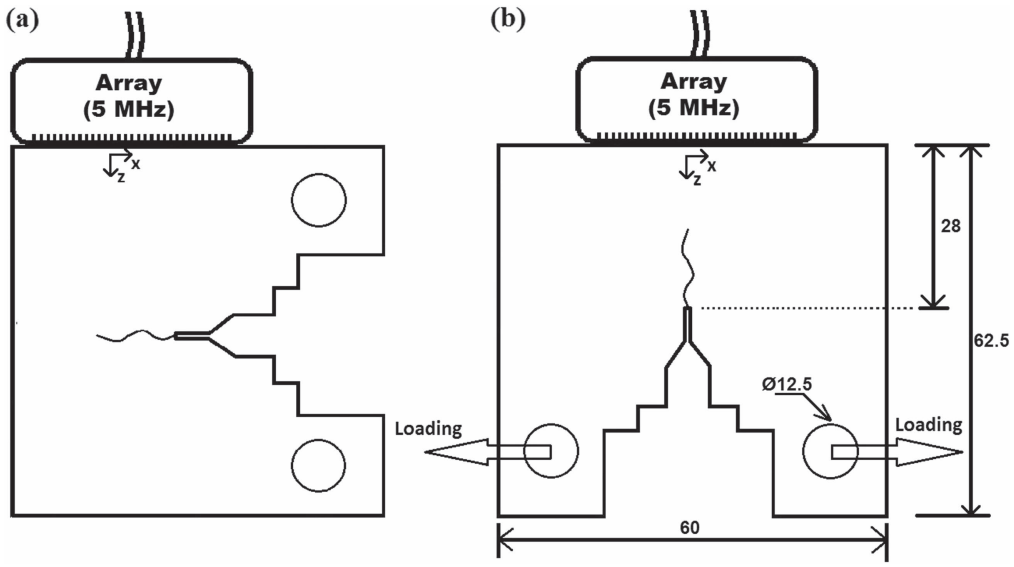

Figure 1. Schematic diagrams of pulse-echo configurations with array placed on (a) the right-hand side and (b) the top of the compact test specimen.

For a general nonlinear defect illuminated by ultrasonic waves, the interaction results in a transfer of energy from the fundamental frequency to subharmonics, superharmonics and modulation frequencies of the incident bandwidth. Regardless of the frequency component that the energy moves to, it is always lost from the transmission bandwidth, resulting in small changes to amplitude and phase of those frequency components. Hence, we now explore the relative difference in amplitude and phase of the transmission bandwidth for parallel and sequentially focused fields. In this study a narrow bandwidth from $\frac{5}{6}\omega_0$ to $\frac{7}{6}\omega_0$ was examined relative to the nominal centre frequency, ω_0. These limits are chosen to effectively measure the remaining waves at the fundamental frequency by minimising the contributions from internal movement of energy within the evaluated bandwidth. Consequently, the received time series in the sequential focusing case, $A_s(t)$, for an N element array is given as

$$A_s(t) = \int_{\frac{5}{6}\omega_0}^{\frac{7}{6}\omega_0} \left(\sum_{m=1}^{N} \left(\sum_{n=1}^{N} F_{n,m}(\omega) \mathrm{e}^{\mathrm{i}\omega\delta_n^T(r)} \right) \mathrm{e}^{\mathrm{i}\omega\delta_m^R(r)} \right) \times \mathrm{e}^{-\mathrm{i}\omega t} \mathrm{d}\omega. \quad (1)$$

Likewise, the amplitude, $A_p(t)$, in the parallel focusing case is calculated as follows

$$A_p(t) = \int_{\frac{5}{6}\omega_0}^{\frac{7}{6}\omega_0} \left(\sum_{m=1}^{N} G_m(\omega) \mathrm{e}^{\mathrm{i}\omega\delta_m^R(r)} \right) \mathrm{e}^{-\mathrm{i}\omega t} \mathrm{d}\omega. \quad (2)$$

Experimental procedure

The effect of fatigue cracks on the time domain responses, $A_s(t)$ and $A_p(t)$ is first examined. Mild steel ASTM A36 ($c = 5924\,\mathrm{m\,s^{-1}}$) compact tension (CT) specimens were manufactured according to the ASTM standard E647-05. The load was varied between 2 and 15 kN in a hydraulic testing machine (Instron 8800MJ6272, UK) to ensure that the specimens failed in the high cycle fatigue regime [23]. This fatigue test was conducted in order to relate linear and nonlinear metrics to the crack size. Furthermore, before the fatigue test, metallographic preparation was performed around the electro-discharge machined (EDM) starter-notch by fine grinding using silicon carbide paper as well as further fine abrasion using polishing cloth with a 3 μm monocrystalline diamond suspension. The microstructure around the crack was then observed by a microscope (Zeiss Axio Imager 2, Germany) and, consequently, the crack length was measured periodically during the fatigue test.

The ultrasonic measurements were implemented through positioning an array on the faces of the CT specimen as shown in figures 1(a) and (b) and operating it in pulse-echo mode. It should be noted that the arrangement in figure 1(a) provides the best case scenario for capturing the fundamental signals reflected from closed cracks since the cracks grown by the cyclic tension present a larger reflecting surface in this orientation. However, we also examine the efficacy of imaging by positioning the array above the cracks in figure 1(b) as this is often the only option in many industrial application scenarios, due to access restrictions. All the measurements were performed with a 64 element ultrasonic array (Imasonic, France) with nominal centre frequency of 5 MHz and pitch of half wavelength, using a commercial array controller (Micropulse, Peak NDT, UK).

As with other amplitude modulation methods, the proposed coherent nonlinear imaging method relies on the presence of backscatter in the vicinity of nonlinear defect in order for the distorted component of the field to be returned to the transducer. This suggests that the nonlinearities cannot be detected until the linear scattering features are formed (i.e. the detection is less sensitive to the very early closed cracks).

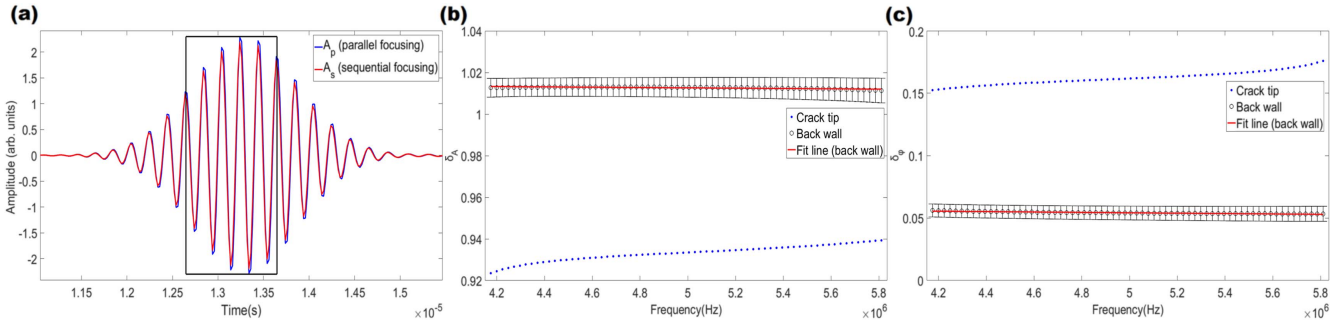

Figure 2. At 30 000 loading cycles, (a) time traces for a pixel at the crack tip. The rectangular box denotes the portion of the signal that was analysed in the frequency domain. (b) Amplitude ratio, δ_A, at crack tip and back wall, and (c) relative phase in radians, δ_φ against frequency at the crack tip and back wall. Note that error bars denote standard deviations of the metrics at multiple linear points selected from back wall at the given frequency.

Therefore, the arrangement in figure 1(a) is particularly beneficial as the orientation allows stronger linear reflections from the cracks. With this arrangement, our proposed technique demonstrated its ability to localise the crack tip and size the cracks throughout the fatigue life. The underlying physics behind the nonlinear image is now explored to understand the nonlinear responses. Two fundamental physical quantities (absolute amplitude and phase), of which the nonlinear image consists, were studied over the considered bandwidth.

Example parallel and sequential time traces produced by focusing at the crack tip in a CT specimen with a crack of length of 695 μm are shown in in figure 2(a). The relative properties of the fields are the analysed in the frequency domain in figures 2(b) and (c) from which is can be seen that the parallel and sequential fields obtained from a pixel at the crack tip show differences in both amplitude and phase. Note that Gaussian windowed signals centred at focal time, t_f in figure 2(a) were post-processed for this frequency analysis.

The amplitude ratio between sequential and parallel focusing is first studied which is defined as

$$\delta_A(\omega) = \frac{|A_s(\omega)|}{|A_p(\omega)|}. \tag{3}$$

Figure 2(b) shows the amplitude ratio over the post-processed frequency band (one third of the centre frequency), form which hit can be seen that the ratio is below unity indicating that the amplitude of the parallel field is higher than that of the sequential field. This finding is somewhat counter-intuitive as it has been previously shown, for example through diffuse energy imaging [22], that the total energy loss from the fundamental component is higher in the parallel transmission case. It is possible that the apparent increase in amplitude is a consequence of interference effects between the distorted and undistorted components of the field. A similar observed amplitude increase has also been observed using the amplitude modulation approach to coherent nonlinear imaging [20]. The relative phase between sequential and parallel focusing is then evaluated as

$$\delta_\varphi(\omega) = \angle A_s(\omega) - \angle A_p(\omega). \tag{4}$$

Figure 2(c) shows that the relative phase when focused at the crack tip increases significantly. For comparison, multiple linear points selected from back wall, considered as undamaged areas, were chosen to understand the background level, and results suggest that all of their relative phases remain at a lower level. The difference in phase and amplitude between the backwall measurements can be attributed to the bulk material nonlinearity, coupling and, more significantly, the nonlinearity of the instrumentation. Nonetheless, the observed differences suggest that the relative phase and amplitude allow for the characterisation and localisation of the nonlinear defect.

Nonlinear coherent imaging (NCI)

Given that it is observed that nonlinear elasticity induces measurable differences in the coherently scattered component of parallel and sequentially focused fields, this is now used a basis for nonlinear imaging. First, the amplitude intensity of the focal point r in the sequential case I_s is given as

$$I_s(x, z) = A_s(t_f). \tag{5}$$

This sequential imaging is equivalent to a conventional linear total focusing method image. Similarly, the intensity of the focal point r in the parallel case I_p is given by

$$I_p(x, z) = A_p(t_f). \tag{6}$$

Finally an image is formed from by calculation of the nonlinear metric ζ at a given imaging/focal point $\zeta(x, z)$ by subtracting the parallel and sequential amplitudes as follows

$$\zeta(x, z) = |I_s(x, z) - I_p(x, z)|. \tag{7}$$

Figures 3(a) and (b) present the sequential and parallel images of the region around the EDM starter-notch tip and fatigue crack. These images, which are linearly equivalent, are seen to be indistinguishable, even in the presence of crack growth. The subtracted image in figure 3(c) is seen to suppress the linear geometric features, revealing the nonlinear response of the fatigue crack with the maximum nonlinearity located close to the crack tip. It is noted that the residual amplitude of the subtracted fields used to form the nonlinear

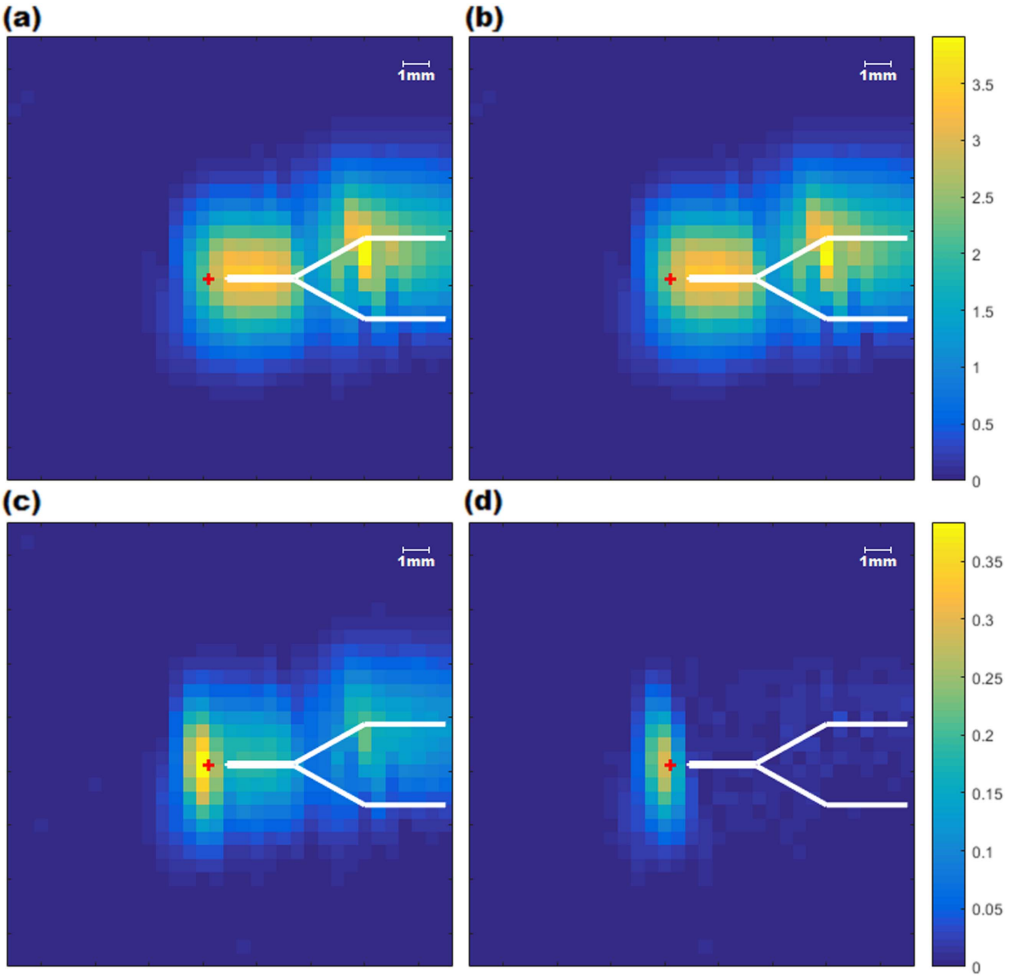

Figure 3. At 30 000 loading cycles, (a) sequential image and (b) parallel image in arbitrary units, (c) image of the nonlinear metric, ζ and (d) image of the nonlinear metric with instrumentation compensation applied, $\hat{\zeta}$. The inspection configuration is as illustrated in figure 1(a). The red cross indicates the micrographically measured crack tip and the geometry of the EDM starter notch is shown with white lines.

image is predominantly from the observed differences in phase rather than amplitude. This is due to small changes in phase producing large residual amplitudes when the responses are subtracted.

Although reduced through subtraction, the suppression of linear features is imperfect. This is a consequence of both the bulk material nonlinearity and that of the instrumentation, specifically the ability of the instrument to produce identical waveforms in both parallel and sequential transmission modes. This was seen in figures 2(b) and (c) as differences in amplitude and phase for fields focused on the specimen back wall which is thought to act as a purely linear reflector. To compensate for these effects, the relative amplitude and phase of the baseline measurements is first averaged for multiple points on the backwall. This baseline response is then approximated through a linear fit in the frequency domain, indicated by the red lines in figures 2(b) and (c). These approximate baseline phase and amplitude terms are denoted $\hat{\delta}_{\varphi}(\omega)$ and $\hat{\delta}_{A}(\omega)$ respectively. The influence of instrument nonlinearity can be removed by applying a correction for the relative phase and amplitude arising from the instrument to the sequential focused amplitude, which as follows

$$\hat{A}_s(\omega) = \frac{A_s(\omega)}{\hat{\delta}_A(\omega)} \mathrm{e}^{-\mathrm{i}\hat{\delta}_{\varphi}(\omega)}, \tag{8}$$

where $\hat{A}_s(\omega)$ denotes the corrected sequential amplitude. An improved image is then obtained by computing the new nonlinear metric $\hat{\zeta}$ with the compensated intensity in the sequential case as follows

$$\hat{\zeta}(x, z) = |\hat{A}_s(t_f) - I_p(x, z)|. \tag{9}$$

Figure 3(d) shows the nonlinear image with the instrumentation compensation from which it can be seen that the background levels drop approximately from 0.2 to 0.02 in nonlinear metric.

Monitoring crack growth

This section examines the response of the coherent nonlinear imaging method for periodic monitoring of crack growth from 0 to 100 000 cycles (*circa* 74% of fatigue life). Here the loading step was chosen as 10 000 cycles in order to allow

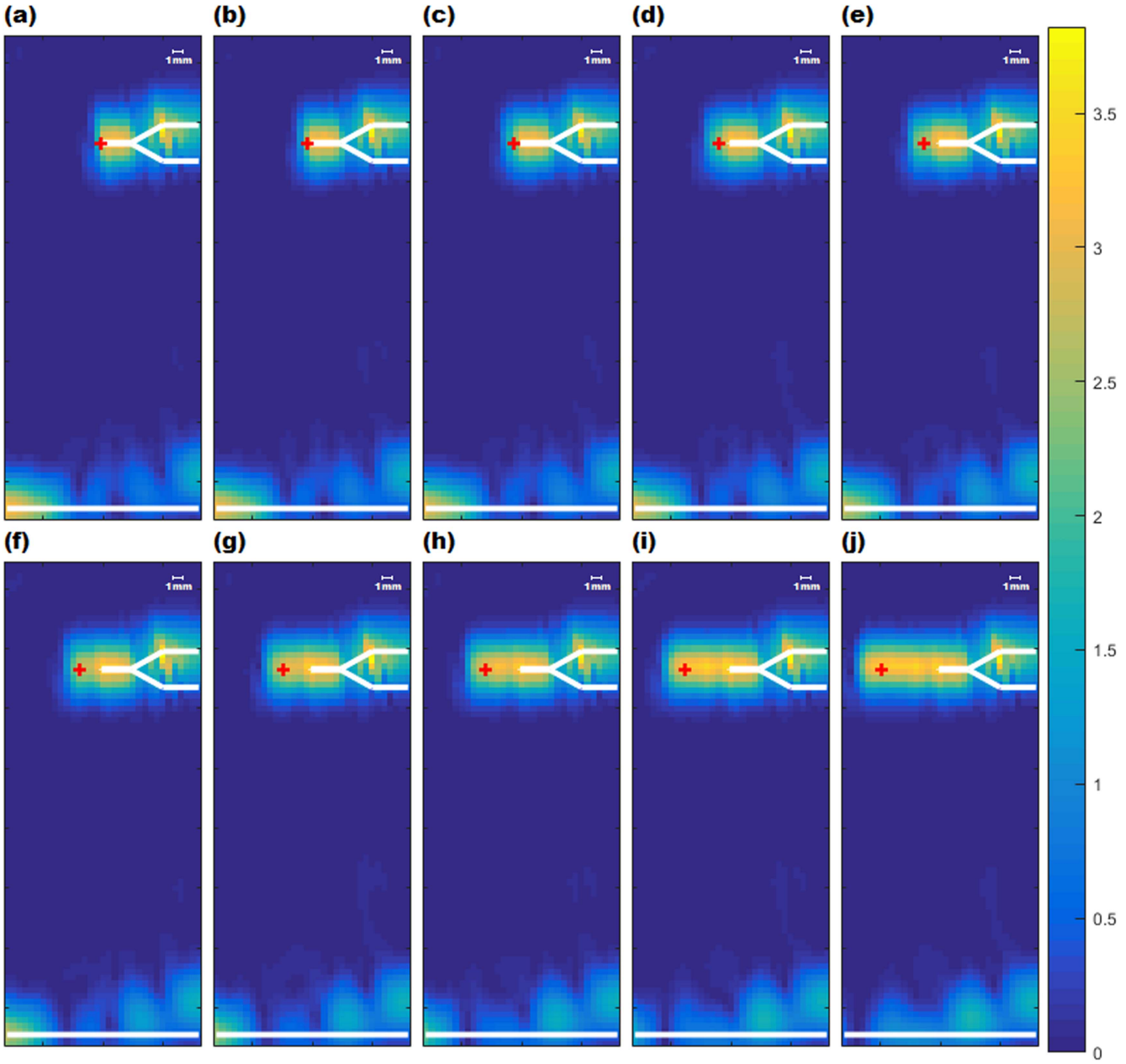

Figure 4. Sequential images in arbitrary units at (a) 10 000 cycles, (b) 20 000 cycles, (c) 30 000 cycles, (d) 40 000 cycles, (e) 50 000 cycles, (f) 60 000 cycles, (g) 70 000 cycles, (h) 80 000 cycles, (i) 90 000 cycles and (j) 100 000 cycles. The inspection configuration is as illustrated in figure 1(a) and the red cross marks the micrographically measured crack tip.

the early stage damage to be monitored and detection performance limits to be investigated. Before conducting the fatigue test, the baseline of relative phase ($\hat{\delta}_\varphi$) and amplitude ratio ($\hat{\delta}_A$) from points across the back wall were evaluated in order to compensate for the instrument nonlinearity as indicated in equations (3) and (4). The baseline parameters, $\hat{\delta}_\varphi$ and $\hat{\delta}_A$, acquired for the 0 cycle case are used in the image formation of each subsequent loading step. Figures 4(a)–(j) show images obtained with sequential imaging (equation (8)) from 10 000 to 100 000 cycles. Before 50 000 cycles, the crack at the early stages are barely detectable due to their small size (maximum 1.3 mm) relative to the fundamental wavelength (1.2 mm). Beyond 50 000 cycles, the cracks are detectable and can be sized from these sequential images.

In contrast, the coherent nonlinear images obtained using equation (9) in figures 5(a)–(j) show sensitivity to cracks as well as high selectivity of nonlinear features at an earlier stage in the fatigue life. The crack was first distinguishable at 20 000 cycles (indicated by a magnitude (0.082) of the nonlinear metric $\hat{\zeta}$ higher by a factor of 2 compared with the background level observed at current and previous stages), which corresponded to a crack length of 0.35 mm. It is worth noting that selectivity of nonlinear defects in these early stages is improved significantly by the instrumentation compensation, without which the uncorrected nonlinear metric, ζ,

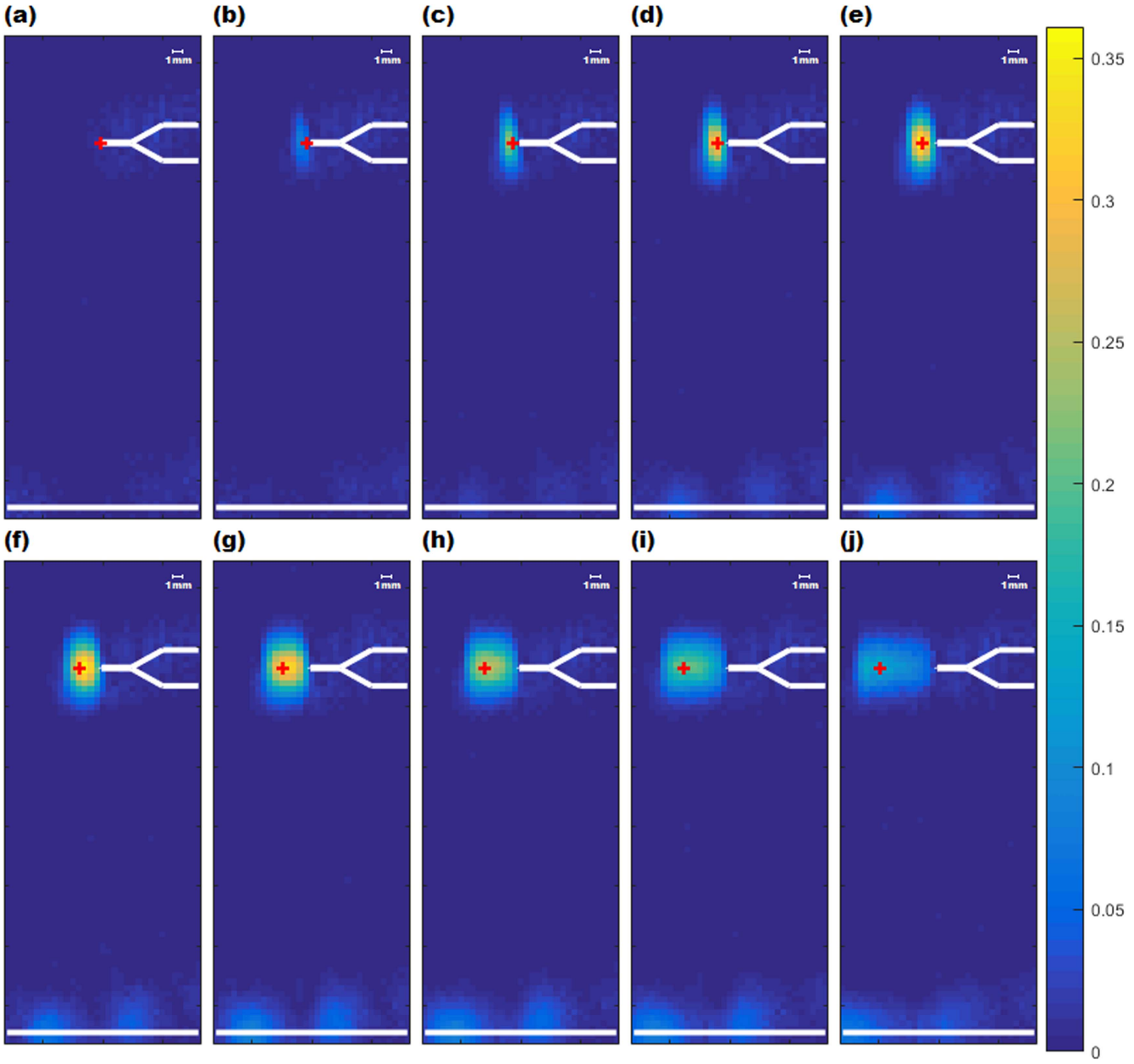

Figure 5. Nonlinear images in nonlinear metric, $\hat{\zeta}$ at (a) 10 000 cycles, (b) 20 000 cycles, (c) 30 000 cycles, (d) 40 000 cycles, (e) 50 000 cycles, (f) 60 000 cycles, (g) 70 000 cycles, (h) 80 000 cycles, (i) 90 000 cycles and (j) 100 000 cycles. The inspection configuration is as illustrated in figure 1(a) and the red cross marks the micrographically measured crack tip.

from cracks was at the same level as those from back wall. Subsequently, the nonlinear metric is seen to increase until 60 000 cycles and then start to decrease gradually. It can be seen that the position of the peak nonlinear metric at each stage is consistently close to the micrographically measured crack tip. Furthermore, the results suggest the crack started to become progressively more open (i.e. the nonlinear metric is decreasing and the linear metric is increasing) from 60 000 cycles, which is consistent with the increased linear amplitude seen in the corresponding linear images in figures 4(b)–(j). This late-life amplitude effect is thought to be due to by fewer contact points across the crack faces leading to reduced instances of nonlinear contact acoustic effects. Note that the change in relative phase δ_φ has a significantly greater effect than the relative amplitude δ_A on the nonlinear imaging metric (before 60 000 cycles), which indicates that the nonlinear phase response is more sensitive to cracks at the early stages.

Figure 6(a) shows the relationship between the maximum nonlinear metric (obtained from the images shown in figure 5) and the loading cycles. The error bars denote the standard deviation across multiple repeat (between 5 and 8) measurements on the same sample and so indicate measurement consistency. Furthermore, four identical specimens were loaded to 30 000 cycles (resulting in crack lengths varying

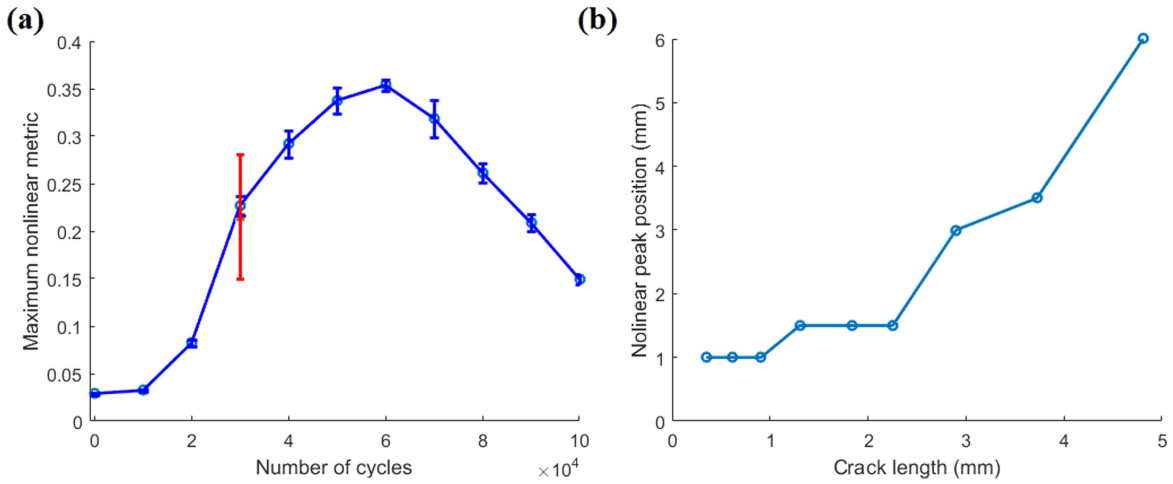

Figure 6. Maximum nonlinear metric $\hat{\zeta}$ during fatigue as a function of (a) number of fatigue cycles (blue and red error bars represent standard deviations of multiple measurements on the single specimen and across five specimens respectively). (b) Measured crack length in mm from the nonlinear image (notch end to position of maximum nonlinear metric γ) during fatigue as a function of micrographically measured crack length in mm.

between 515 and 750 μm) and their measured maximum nonlinear metrics are shown as the red point in figure 6(a). Their mean and standard deviation are calculated over all specimens using 5 repeat measurements on each sample. This then provides some indication of the repeatability between different specimens, but is thought primarily to reflect the statistical variance of crack growth between samples. Also, figure 6(b) shows its ability to predict the location of the crack tip from 20 000 cycles (the starting point where the crack of 0.35 mm was detectable).

Dependence on linear scattering

Inspections performed in which the array insonifies the crack face at normal incidence, as illustrated in figure 1(a), are particularly well suited to the presented coherent nonlinear imaging method because the specular reflection from the crack face allows the nonlinear information contained in the wave to be returned to the receiver. Naturally, due to access limits, such a configuration is not always possible and consequently it is important to evaluate performance for less favourable inspection angles. To this end, imaging was performed with the array positioned such that it predominantly insonifies the crack tip as illustrated in figure 1(b). Sequential and coherent nonlinear images for 0 and 100 000 cycles are shown in figure 7. Figure 7(a) shows that the magnitude around the starter-notch in the linear sequential image is approximately 10% of those from the geometric features. As the crack grows, the signals reflected from the EDM starter-notch become even weaker as the transmitted signals are first diffracted by the crack tip. Additionally, the crack tip itself is seen to exhibit only very weak linear scattering. Figure 7(d) shows that at 100 000 cycles, the NCI shows a feature at the starter-notch tip that is not seen at 0 cycles (i.e. figure 7(c)). This is thought to be due to the incident field being nonlinearly distorted by the crack and then subsequently being linearly scattering by the starter-notch tip. No features within the coherent nonlinear image are seen to correspond to the crack tip for this inspection angle, meaning that although there is some indication of a nonlinear feature, no defect sizing is information is provided.

To confirm that the observed reduced performance of the coherent nonlinear method due to an unfavourable incident angle is a consequence of the reduced linear scattering as opposed to a reduction in the nonlinear response at this inspection angle, results are also obtained using the nonlinear diffuse energy imaging method. Nonlinear diffuse energy imaging is a technique which is independent of local linear scattering and consequently can be used to separate the nonlinear response of the defect. The nonlinear diffuse energy imaging method is implemented with the same experimental apparatus using a time domain window length of 0.12 ms with the reception start time at 0.1 ms (see [23] for fuller details of this method). Nonlinear diffuse energy images for 0 and 100 000 cycles are shown in figures 7(e) and (f) respectively. It can be clearly seen that there is a nonlinear response that is coincident with the location of the fatigue crack and not the location of the starter-notch tip. This confirms that nonlinear distortion of the field still occurs from this inspection angle. From this investigation it is apparent that it is the absence of strong linear scattering in the vicinity of the defect that reduces detectability using the coherent nonlinear method. These results support the hypothesis that coherent nonlinear imaging methods rely on the convolution of nonlinear distortion with the linear scattering response of defects. While it is clear that the necessity for linear scattering close to the inspection point represents a distinct disadvantage in comparison to nonlinear diffuse energy imaging, the lack of a requirement for a measurable diffuse state makes this coherent imaging approach more widely applicable in practice.

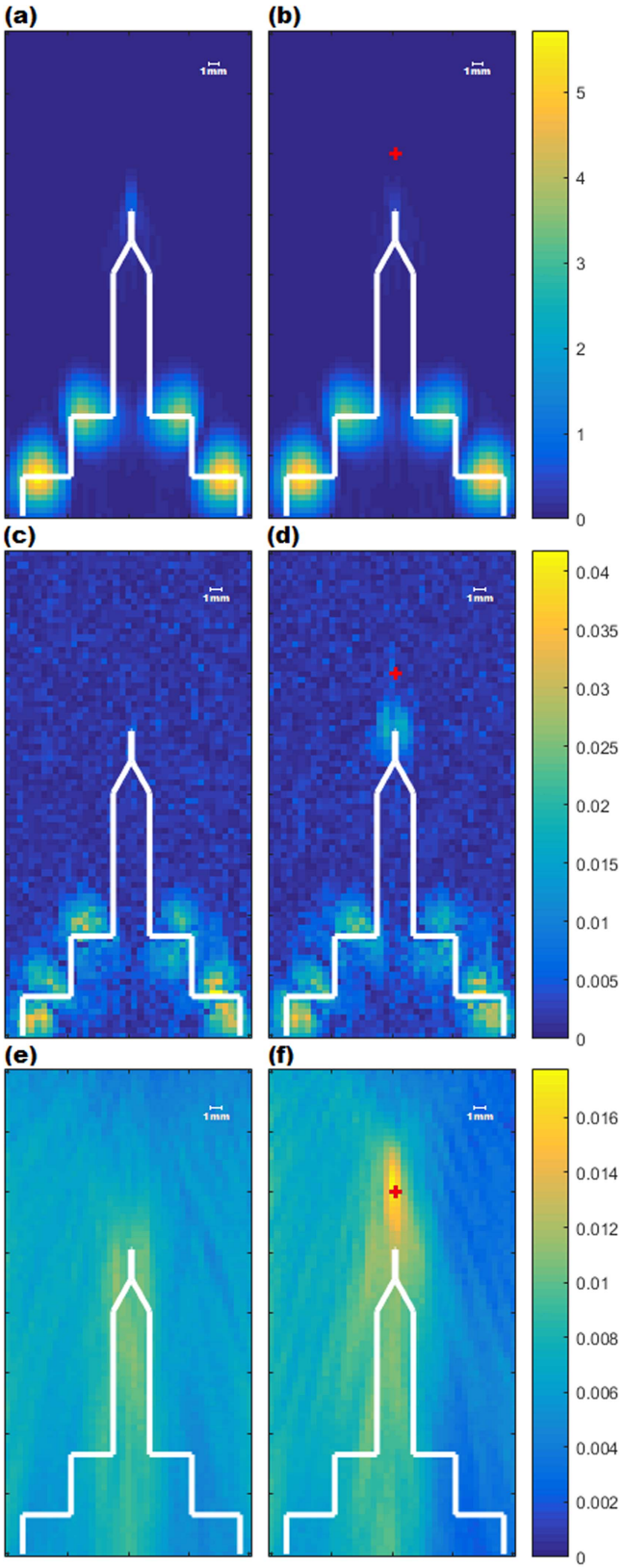

Figure 7. Linear sequential images in arbitrary units, at (a) 0 cycle and (b) 100 000 cycles. Nonlinear images in nonlinear metric, $\hat{\zeta}$ at (c) 0 cycle and (d) 100 000 cycles. Nonlinear diffuse energy images (e) 0 cycle and (f) 100 000 cycles. The inspection configuration is as illustrated in figure 1(a) and the red cross marks the micrographically measured crack tip.

Conclusions

A form of coherent nonlinear ultrasonic imaging was proposed to effectively localise and quantify the extent of cracking by evaluating differences in parallel and sequentially focused fields. The linear sequential and parallel images reveal essentially geometric information from sample boundaries and large defects, whereas the coherent nonlinear images reveal nonlinear features such as partially-closed cracks and crack tips. The ability of NCI to effectively monitor fatigue crack growth has been demonstrated on fatigue cracking in mild steel from a crack length of 350 μm (*circa.* 15% of fatigue life). Localisation of the crack tip was realisable by observing the peak nonlinear metric with an accuracy of less than 1 mm. Further, it was shown that significant improvements in linear feature suppression can be achieved through appropriate compensation for instrumentation nonlinearity, providing the ability to better distinguish the nonlinear defect from other geometric (i.e. linear) features. By studying the influence of inspection angle, in conjunction with diffuse nonlinear measurements, evidence was provided to show that the performance of coherent nonlinear imaging methods is dependent on the convolution of nonlinear distortion with the linear scattering response of defects.

This reliance of linear scattering is a limitation of the technique not present for nonlinear diffuse energy imaging. However, the principal disadvantage to the nonlinear diffuse energy technique is the necessity for a measurable diffuse state. This prevents the applicability to large structures and highly attenuating materials, for which the signal amplitude would become immeasurable by the time a diffuse state is formed. Consequently, it is unlikely to be effective in heavy industry applications. Such situations necessitate the use of the early-time, coherent component of the field instead. Consequently, despite the observed limitations, the NCI technique considered here is practically more widely applicable than nonlinear diffuse energy imaging.

Acknowledgments

This works was supported through the core research program within the UK Research Centre in NDE (RCNDE) funded by the Engineering and Physical Sciences Research Council (EPSRC, grant number EP/L022125/1). Data necessary to support the conclusions are included in the paper.

ORCID iDs

Jingwei Cheng https://orcid.org/0000-0002-7129-4865

References

[1] Nagy P B 1998 Fatigue damage assessment by nonlinear ultrasonic materials characterization *Ultrasonics* **36** 375–81

[2] Matlack K H, Kim J-Y, Jacobs L J and Qu J 2015 Review of second harmonic generation measurement techniques for material state determination in metals *J. Nondestruct. Eval.* **34** 273
[3] Solodov I Y 1998 Ultrasonics of nonlinear contacts: propagation, reflection and NDE-applications *Ultasonics* **36** 383–90
[4] Solodov I, Krohn N and Busse G 2002 Can: an example of nonclassical acoustic nonlinearity in solids *Ultraonics* **40** 621–5
[5] Solodov I, Wackerl J, Pleiderer K and Busse G 2004 Nonlinear self-modulation and subharmonic acoustic spectroscopyfor damage detection and local *Appl. Phys. Lett.* **84** 5386–8
[6] Su Z, Zhou C, Hong M, Cheng L, Wang Q and Qing X 2014 Acousto-ultrasonics-based fatigue damage characterization: linear versus nonlinear signal features *Mech. Syst. Signal Process.* **45** 225–39
[7] Lim H J, Song B, Park B and Sohn H 2015 Noncontact fatigue crack visualization using nonlinear ultrasonic modulation *NDT&E Int.* **73** 8–14
[8] Fierro G P M and Meo M 2015 Residual fatigue life estimation using a nonlinear ultrasound modulation method *Smart Mater. Struct.* **24** 025040
[9] Lim H J and Sohn H 2015 Fatigue crack detection using structural nonlinearity reflected on linear ultrasonic features *J. Appl. Phys.* **118** 244902
[10] Amura M, Meo M and Amerini F 2011 Baseline-free estimation of residual fatigue life using a third order acoustic nonlinear parameter *J. Acoust. Soc. Am.* **130** 1829–37
[11] Kim J-Y, Jacobs L J, Qu J and Littles J W 2006 Experimental characterization of fatigue damage in a nickel-base superalloy using nonlinear ultrasonic wave *J. Acoust. Soc. Am.* **120** 1266–73
[12] Cantrell J H and Yost W T 2001 Nonlinear ultrasonic characterization of fatigue microstructures *Int. J. Fatigue* **23** 487–90
[13] Solodov I, Wackerl J, Pfleiderer K and Busse G 2004 Nonlinear self-modulation and subharmonic acoustic spectroscopy for damage detection and location *Appl. Phys. Lett.* **84** 5386–8
[14] Croxford A J, Wilcox P D, Drinkwater B W and Nagy P B 2009 The use of non-collinear mixing for nonlinear ultrasonic detection of plasticity and fatigue *J. Acoust. Soc. Am.* **126** 117–22
[15] Ohara Y, Horinouchi S, Hashimoto M, Shintaku Y and Yamanaka K 2010 Nonlinear ultrasonic imaging method for closed cracks using subtraction of responses at different external loads *Ultrasonics* **51** 661–6
[16] Yan Z and Nagy P B 2000 Thermo-optical modulation for improved ultrasonic fatigue crack detection in Ti–6Al–4V *NDT&E Int.* **33** 213–23
[17] Jiao J P, Drinkwater B W, Neild S A and Wilcox P D 2009 Low-frequency vibration modulation of guided waves to image nonlinear scatters for structural health monitoring *Smart Mater. Struct.* **18** 065006
[18] Ohara Y, Takahashi K, Ino Y, Yamanaka K, Tsuji T and Mihara T 2017 High-selectivity imaging of closed cracks in a coarse-grained stainless steel by nonlinear ultrasonic phased array *NDT&E Int.* **91** 139–47
[19] Ohara Y, Mihara T, Sasaki R, Ogata T, Yamamoto S, Kishimoto Y and Yamanaka K 2007 Imaging of closed cracks using nonlinear response of elastic waves at subharmonic frequency *Appl. Phys. Lett.* **90** 011902
[20] Ikeuchi M, Jinno K, Ohara Y and Yamanaka K 2013 Improvement of closed crack selectivity in nonlinear ultrasonic imaging using fundamental wave amplitude difference *Japan. J. Appl. Phys.* **52** 07HC08
[21] Haupert S, Renaud G and Schumm A 2017 Ultrasonic imaging of nonlinear scatters buried in a medium *NDT&E Int.* **87** 1–6
[22] Potter J N, Croxford A J and Wilcox P D 2014 Nonlinear ultrasonic phased array imaging *Phys. Rev. Lett.* **113** 144301
[23] Cheng J, Potter J N, Croxford A J and Drinkwater B W 2017 Monitoring fatigue crack growth using nonlinear ultrasonic phased array imaging *Smart Mater. Strct.* **26** 055006